Научно-технический вестник Брянского государственного университета, 2025, №4
Nauchno-tekhnicheskiy vestnik Bryanskogo gosudarstvennogo universiteta, 2025, No.4
DOI: 10.22281/2413-9920-2025-11-04-470-486

УДК (UDC) 629.5:629.52

УЛУЧШЕНИЕ ПРОГНОЗИРОВАНИЯ ДЕМПФИРОВАНИЯ КРЕНА: НОВЫЙ ПОДХОД С ПРОВЕРКОЙ МЕТОДОВ LWM И AGM

ENHANCING ROLL-DAMPING PREDICTIONS: A NOVEL APPROACH WITH LWM AND AGM VALIDATION

Назаризаде К.
K. Nazarizadeh

Бабольский технологический университет имени Ноширвани (Бабол, Иран)
Babol Noshirvani University of Technology (Babol, Iran)

Аннотация. *Демпфирование крена является главной проблемой остойчивости крупных морских судов, особенно перевозчиков сжиженного природного газа и плавучих установок для добычи, хранения и отгрузки нефти и газа, которые оснащены большими сферическими резервуарами, где разбрызгивание жидкости может усилить качку. В данной статье для улучшения прогнозирования угла крена представлен гибридный вейвлет-подход. Был построен многослойный персептрон (MLP) на языке прогнозирования Python, который был интегрирован с вейвлет–методом Лукаса (LWM) с целью создания модели MLP-LWM, способную описывать нелинейную динамику крена. Комбинированный метод полностью соответствовал наблюдаемому поведению (R2 = 0,998010) и был проверен на соответствие установленным методикам, включая метод Акбари-Ганджи (AGM). Для репрезентативного испытания на крен под углом 4° метод AGM продемонстрировал наиболее полное соответствие эталонному показателю, получив среднее значение θ = 0,0528 и стандартное отклонение 0,0146. Метод гомотопических возмущений (HPM) показал незначительную погрешность в 0,87%, тогда как метод MLP–LWM дал большую погрешность в 5,11%, при среднем значении θ = 0,0555 и стандартном отклонении 0,0154. Сравнение временных рядов показывает, что все методы фиксируют один и тот же общий тренд затухания, но MLP-LWM лучше справляется с более мелкими переходными процессами, чем HPM. Эти результаты показывают, что гибридный подход является многообещающим для определения сложных явлений демпфирования, связанных с расплескиванием, однако для достижения постоянной точности AGM требуются дополнительные обучающие данные и настройка гиперпараметров. Таким образом, модель MLP–LWM предлагает гибкую альтернативу с высоким разрешением для прогнозирования изменения крена на судах, чувствительных к качке, при условии проведения дополнительной калибровки перед эксплуатационным использованием. Будущая работа будет сосредоточена на расширении учебных наборов данных, полученных на основе различных состояний моря и геометрии резервуаров, систематическом поиске гиперпараметров и проверке в реальных условиях с*

Abstract. *Roll damping is a central stability concern for large maritime vessels, especially LNG carriers and FPSOs fitted with large spherical tanks, where liquid sloshing can intensify motions. This study introduces a hybrid data-driven wavelet approach to improve roll-angle prediction. We built a multilayer perceptron (MLP) in Python and integrated it with the Lucas wavelet method (LWM) to create an MLP–LWM model capable of modeling nonlinear roll dynamics. The combined method delivered a strong fit to observed behaviour (R^2 = 0.998010) and was validated against established techniques, including Akbari-Ganji's Method (AGM). For a representative 4° roll test, AGM produced the closest agreement with reference behaviour, yielding mean θ = 0.0528 and standard deviation 0.0146. The homotopy perturbation method (HPM) showed a minor error of 0.87%, whereas the MLP–LWM produced a larger error of 5.11%, with mean θ = 0.0555 and standard deviation 0.0154. Time-history comparisons reveal that all methods capture the same overall decay trend, but MLP–LWM resolves finer transient features better than HPM. These results indicate that the hybrid approach is promising for capturing complex sloshing-related damping phenomena, yet it requires additional training data and hyperparameter tuning to reach the consistent accuracy of AGM. In summary, MLP–LWM offers a flexible, high-resolution alternative for roll-damping prediction in sloshing-sensitive ships, provided that further calibration is undertaken before operational use. Future work will focus on expanding training datasets drawn from varied sea states and tank geometries, systematic hyperparameter searches, and real-world validation with model tests or full-scale measurements to close the performance gap urgently.*

DOI: 10.22281/2413-9920-2025-11-04-470-486

помощью модельных тестов или полномасштабных измерений.
Ключевые слова: *демпфирование крена, MLP, вейвлет-метод Лукаса, HPM, AGM.*

Дата получения статьи: *11.09.2025*
Дата принятия к публикации: *09.10.2025*
Дата публикации: *25.12.2025*

Сведения об авторе:
Кимия Назаризаде – магистр по направлению «Военно-морская архитектура и проектирование конструкций кораблей», военно-морской архитектор, научный сотрудник факультета машиностроения Бабольского технологического университета имени Ноширвани,
e-mail: k.nazarizadeh@outlook.com
ORCID: https://orcid.org/0009-0008-5383-761X

Keywords: *Roll-damping, MLP, Lucas Wavelet Method, HPM, AGM.*

Date of manuscript reception: *11.09.2025*
Date of acceptance for publication: *09.10.2025*
Date of publication: *25.12.2025*

Author' information:
Kimia Nazarizadeh – M.Sc. Naval Architecture and Ship Structural Design, Naval Architect, Research Assistant, Department of Mechanical Engineering, Babol Noshirvani University of Technology,
e-mail: k.nazarizadeh@outlook.com
ORCID: https://orcid.org/0009-0008-5383-761X

NOMENCLATURE

ϑ	- Time, s
θ	- Roll angle, degrees
$\dot{\theta}$	- Angular velocity, degrees/s
$\ddot{\theta}$	- Angular acceleration, degrees/s^2
I_{44}	- Mass moment of inertia, kg/m^2
A	- Added mass moment of inertia, kg/m^2
B_1	- Linear damping
B_2	- Nonlinear damping
LBP	- Length between perpendicular
D	- Draft
M	- Displacement, m^3
$M(t)$	- Exciting moment, N·m
GZ	- Righting lever of the ship, m
$\overline{GM}$	- Metacentric height, m
C	- Restoring coefficient, N/m
ξ	- The ratio of linear damping
η	- Non-dimensional nonlinear term
ι	- Imaginary unit
B	- Breadth
H	- Height of the ship

1. INTRODUCTION

The study of ship roll-damping is a critical area of marine engineering, particularly for vessels such as Liquefied Natural Gas (LNG) carriers, Floating Production Storage and Offloading units (FPSOs), and other ships equipped with large spherical tanks. The significance of roll-damping lies in its ability to stabilise lateral motion, which is essential for ensuring operational safety and efficiency in marine environments. The roll motion of ships is inherently nonlinear, necessitating the application of advanced mathematical methods to solve the governing equations effectively.

Roll-damping mechanisms are vital for maintaining the stability of vessels in the face of external disturbances, such as waves and wind. For LNG carriers, which transport highly volatile cargo, maintaining stability is paramount to prevent accidents and ensure safe operations. The roll motion can lead to significant lateral forces that may compromise the structural integrity of the vessel and its cargo. FPSOs, which are often deployed in harsh marine environments, also face challenges related to roll motion. The large spherical tanks used in these vessels can exacerbate roll dynamics due to their shape and the distribution of mass, making effective roll-damping solutions critical for operational safety.

The roll motion of ships is characterised by its non-linear nature, which complicates the analysis and modeling of roll-damping systems. Non-linear dynamics can lead to unpredictable behaviour, such as capsizing or excessive rolling, which can be detrimental to both the vessel and its cargo. As such, understanding and mitigating roll motion through effective damping mechanisms is essential. Various methods have

DOI: 10.22281/2413-9920-2025-11-04-470-486

been developed to address the non-linear characteristics of roll motion, including numerical simulations and analytical techniques that can provide insights into the complex interactions between ship dynamics and environmental forces [1].

Different methods for predicting ship roll-damping at forward speed, including a simple method and a component analysis considering various damping sources. Formulas derived from theoretical and experimental considerations and a computer program were presented [2]. The generalised Krylov–Bogoliubov asymptotic method was used to develop a nonlinear roll motion model for ships, introducing nonlinearities through damping and restoring terms, with validation through a numerical example for a small vessel [3]. A nonlinear equation describing a ship rolling in synchronous beam waves was proposed. The study employed the generalised Duffing's method in the frequency domain [4].

Another study addressed the complexity of ship roll motion, emphasising the crucial role of accurate estimation of viscous roll-damping, especially due to low potential wave damping. The study offers an extensive literature review on various prediction methods for viscous roll-damping and presents a state-of-the-art estimation method for ship-shaped structures. The developed computer code is validated against experimental data, aiming to provide a comprehensive reference for future research on this topic [5].

The estimation of parameters for ship roll-models has been extensively discussed in recent years, utilising various computational methods, such as theoretical analysis, model experiments, and numerical simulations. Prior research has focused mainly on analytical or numerical approaches to solving the nonlinear roll response of a floating body [6-8]. Nonlinear and fractional differential equations have also been used to investigate roll characteristics [9, 10].

Approximated solutions were obtained by either semi-analytical or numerical methods, while the exact ones are not attainable. Analysing natural roll decay, either numerically or experimentally, can be used to determine the parameters of nonlinear systems. A combination of asymptotic methods such as RKM, HPM, cargo methods, Froude energy, and wavelet methods, is effective for solving nonlinear differential equations [11-13]. The definitions of the natural roll decay allow for the determination of parameters in the nonlinear system.

In the broader field of non-linear equation solutions, various analytical methods have been employed to address the complexities of non-linear fluid dynamics, but roll-damping mechanisms in ship and offshore structures were not studied specifically. Among these methods, Akbari-Ganji's Method (AGM), Homotopy Perturbation Method (HPM), and Variational Iteration Method (VIM) were chosen for this study. They stand out due to their effectiveness in tackling complex nonlinear equations.

The Akbari-Ganji's Method (AGM) is a semi-analytical technique that has been successfully applied to solve a variety of non-linear differential equations. This method involves transforming the non-linear equations into a series of linear equations, which can then be solved iteratively. The AGM is particularly useful in fluid mechanics for problems where traditional analytical methods may fail due to the complexity of the non-linear terms present in the governing equations [14, 15]. Its application in magneto-hydrodynamics (MHD) and non-Newtonian fluid dynamics has demonstrated its versatility and robustness in yielding accurate solutions [16, 17].

The Homotopy Perturbation Method (HPM) is another powerful tool for solving nonlinear equations. Developed by Ji-Huan He, HPM combines the concepts of homotopy and perturbation techniques to construct a solution that converges to the exact solution of the non-linear problem. This method is particularly advantageous as it does not require a small parameter, making it applicable to a broader range of problems, including those in fluid mechanics, where non-linearities are significant [18, 19]. The HPM has been effectively utilised to solve various fluid flow problems, including those involving nanofluids and MHD flows, showcasing its adaptability and efficiency [20, 21].

Wavelet analysis, utilising natural roll decay, offers an efficient approach for estimating ship roll-model parameters. The method’s foun-

DOI: 10.22281/2413-9920-2025-11-04-470-486

dation lies in a smooth orthonormal basis, derived from a mother wavelet, which is pivotal for compression algorithms. Wavelets are distinguished by features such as compact support and multi-resolution analysis, making them highly relevant in both theoretical and practical contexts. They enable the algebraic representation of problems in the wavelet domain, which can be inversely transformed to achieve solutions. With the capability to represent signals concurrently in time and frequency domains, wavelets provide benefits like discrete time-frequency localisation, adaptability, and robustness. They are particularly useful in numerical approximations for solving ordinary and partial differential equations, as well as integral and integrodifferential equations, through various wavelet forms such as Haar, Legendre, Chebyshev, Lucas, and Vieta-Lucas [22-25].

Wavelets are versatile, finding use in various disciplines including mathematics, physics, chemistry, biology, engineering, statistics, and time series analysis. Various wavelet forms and approximation functions are utilised for numerical solutions to initial and boundary value problems. Additionally, wavelet neural networks are gaining recognition as a novel method for addressing nonlinear differential equations [26-28].

2. METHODOLOGY

It should be mentioned that the methodology, including equation solving, compter-based replica, and model development, was conducted using Python for computational efficiency and reproducibility.

2.1. Case Study (I): LNG carrier with two spherical tanks

We have conducted a study on a barge-style vessel, 200 m in length and 46 m in beam, with a focus on its roll response and sloshing issues. The details of this vessel are provided in Table 2. It has a uniform cross-section along its length and is designed to display roll characteristics typical of a Moss-type LNG carrier. The vessel's sloshing effects are simulated using two spherical tanks.

The study was carried out using a computerized model that replicates the conditions of an LNG carrier during side-by-side offloading. We chose a standard load condition of 50% by volume as the reference for this study, with details provided in Table 1 for both the full-scale and the replica scale.

Table 1

Properties of the investigated barge-style LNG carrier[7]

Ship Designation Parameters	Values
LBP, m	200
B, m	46
H, m	25.5
Draught – average, m	11.1
Displacement, kg	99297900
Radius of roll gyration, m	19.4
Radius of pitch gyration, m	68.5

The replica under investigation is depicted in Fig. 1. The vessel's conditions under investigation include calm water and wave conditions. Decay tests were performed in calm water to obtain decay curves. In these tests, the vessel is tilted to an initial angle (as shown in Fig. 2), released when the target is reached, and then allowed to move freely in the calm water [29].

2.2. Case Study (II): FPSO unit

A Floating Production Storage and Offloading (FPSO) unit, representative of Brazilian oil production platforms, serves as the subject of this case study, analyzing two distinct operational loading conditions: full and standard loading. Table 3. presents the primary characteristics of the FPSO under these loading conditi-

DOI: 10.22281/2413-9920-2025-11-04-470-486

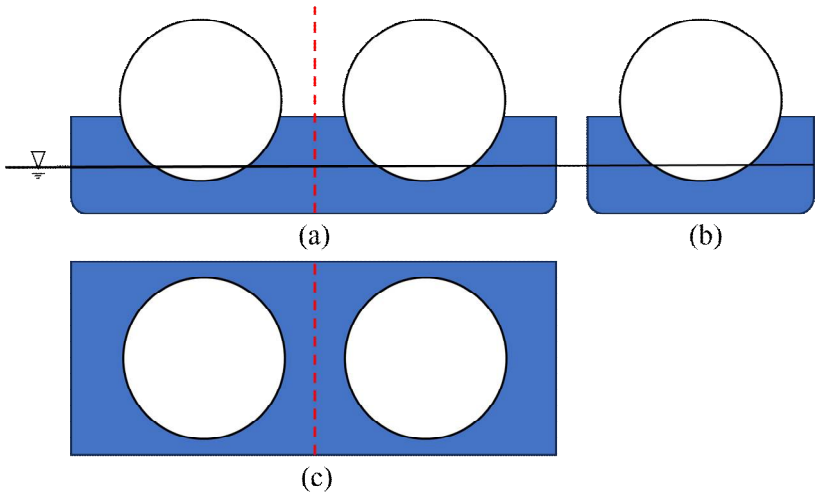

Figure 1. The three-view breakdown drawing of the barge-style LNG carrier

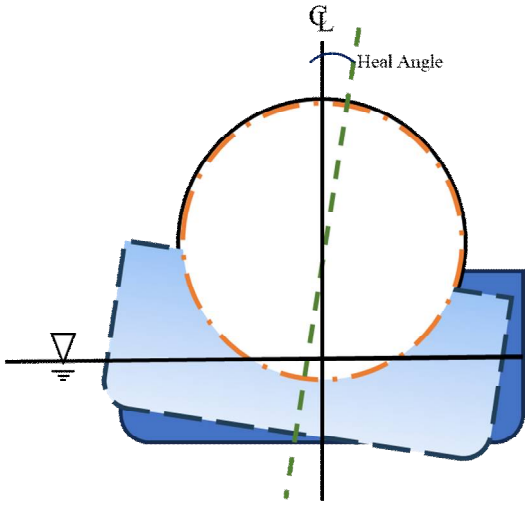

Figure 2. The demonstration of roll decay damping of the vessel in calm water

ons. Across all three loading scenarios, the FPSO featured bilge keels measuring 1.00 m in width, extending along 127.2 m on both sides of the parallel body—an inclusion typical for FPSO units, often with larger dimensions than conventional ships. The average damped roll natural periods of the replica were 14.8 s, and 14.4 s, respectively for the full and standard loading conditions. The estimation of roll decay damping coefficients based on the replica is provided in subsequent table 2 [29].

2.3. Formulating the mathematical models

Two mathematical models are formulated for maritime structures: an LNG carrier with two spherical tanks and an FPSO replica. For the LNG carrier, equations describing roll motion are simplified using Fourier series expansion, while the FPSO replica utilizes a single degree of freedom equation incorporating both linear and quadratic damping components. These formulations are crucial for understanding the behavior of these vessels in different environmental conditions.

2.4. LNG carrier with two spherical tanks

The equations are taken from the referred articles[6, 30, 31].

A ship, taking allows:

$$(M + A)\ddot{\theta} + B_1\dot{\theta} + B_2\dot{\theta}|\dot{\theta}| + C\theta = 0 \quad (1)$$

To determine the linear damping term B1 and the nonlinear damping term B2 in the roll motion equation (Eq. 1), it is assumed that the decaying oscillation exhibits a reasonably harmonic behavior over each half cycle. As a result, the nonlinear term is approximated a linearized using a Fourier series expansion as:

DOI: 10.22281/2413-9920-2025-11-04-470-486

Table 2

Properties of the investigated FPSO unit

Ship Designation Parameters	Standard	Full
LBP, m	320	320
B, m	54.5	54.5
D, m	27.8	27.8
Draught – average, m	14.7	8.0
Displacement, kg	211.884	111.400
Roll inertia, t.m^2	8.29E+07	5.09E+07
Metacentric height, m	9.5	12.41

$$\dot{\theta}|\dot{\theta}| = \frac{8}{3\pi}\omega_n\theta_i\dot{\theta} \quad (2)$$

By substituting in (Eq. 2), the non-dimensional form of the nonlinear equation of motion (Eq. 1), with an initial heel angle of 4° can be expressed as:

$$\ddot{\theta} + 2\xi\omega_n\dot{\theta} + \frac{8}{3\pi}\omega_n\theta_i\dot{\theta} + \omega_n^2\theta = 0 \quad (3)$$

2.5. The FPSO replica

The equations are taken from the referred articles [10, 31].

The equation describing the roll decay motion of shining calm water can be expressed as a single degree of freedom (1-DOF) equation:

$$(I_{44} + a_{44})\ddot{\theta} + b_{44}(\theta)\dot{\theta} + C\theta = 0 \quad (4)$$

The damping coefficient, denoted as $b_{44}(\theta)$, i the equation. The canonical form of (Eq. 4) is defined by:

$$\ddot{\theta} + b(\theta)\dot{\theta} + \omega_n^2\theta = 0 \quad (5)$$

Where:

$$(\theta) = \frac{b_{44}(\theta)}{(I_{44}+a_{44})} \text{ and } \omega_n^2 = \frac{mgGM}{(I_{44}+a_{44})}$$

The damping moment can also be expressed as a combination of linear and quadratic components:

$$b(\theta)\dot{\theta} = b_1\dot{\theta} + b_2\dot{\theta}|\dot{\theta}| \quad (6)$$

By substituting (Eq. 6) into (Eq. 5), we can derive the equation for the ship's roll motion:

$$\ddot{\theta} + b_1\dot{\theta} + b_2\dot{\theta}|\dot{\theta}| + \omega_n^2\theta = 0 \quad (7)$$

2.6. Lucas wavelet method combination with a multi-layer perceptron

In brief, wavelets are small waves constructed from the dilation and translation of a single function, known as the mother wavelet. Lucas wavelets are a specific type, defined by Lucas polynomials, and can be used for function approximation. The Multi-Layer Perceptron (MLP) is a feed-forward artificial neural network employed for tasks like time-series forecasting. In the context of wavelets, MLPs can utilize wavelet solutions as inputs for forecasting tasks, achieving accurate predictions by processing historical data effectively.

2.6.1. Wavelet

A wavelet is a small wave that consists of a collection of functions constructed from the dilation and translation of a single function known as the mother wavelet[32]. This collection of continuous wavelets is defined by:

$$\psi_{a,b}(\vartheta) = |a|^{-\frac{1}{2}}\varphi\left(\frac{\vartheta-b}{a}\right), a, b \in R \text{ and } a \neq 0 \quad (8)$$

Here, $'a'$ represents the dilation parameter and $'b'$ represents the translation parameter. If we assign discrete values to these parameters as $a = a_0{}^{-p}$ and $b = qb_0a_0{}^{-p}$, where $a_0 > 1$ and $b_0 > 0$, and p and q are positive integers, then the family of discrete wavelets is defined as follows:

$$\psi_{p,q}(\vartheta) = |a|^{-\frac{1}{2}}\varphi(a_0{}^p\vartheta - qb_0) \quad (9)$$

2.6.2. Lucas polynomials

The equations are taken from the referred article[33].

The Lucas polynomials of degree q, denoted as L_q, can also be defined using the following relation:

DOI: 10.22281/2413-9920-2025-11-04-470-486

$$L_q(\vartheta) = 2^{-q}[(\vartheta - \sqrt{(\vartheta^2+4)})^q + (\vartheta + \sqrt{(\vartheta^2+4)})^q] \quad (10)$$

Alternatively,

$$L_q(\vartheta) = L_q(2sinh\theta) = \begin{cases} 2\sinh q\theta, & q \text{ is odd} \\ 2\cosh q\theta, & q \text{ is even,} \end{cases} \quad (11)$$

Some of these Lucas polynomials are defined as follows:

$$L_0(\vartheta) = 2, L_1(\vartheta) = \vartheta, L_2(\vartheta) = \vartheta^2 + 2 \text{ and } L_3(\vartheta) = \vartheta^3 + 3\vartheta \text{ and so on...} \quad (12)$$

2.6.3. Lucas wavelet

The equations are taken from the referred articles [8, 33].

Lucas wavelets denoted as $\varphi_{p,q}(\vartheta)$ or $\varphi(k,p,q,\vartheta)$ are defined on the interval [0, 2) with four arguments:

$$\varphi_{p,q}(\vartheta) = \begin{cases} 2^{\frac{k+1}{2}}\widetilde{L_q}(2^{k+1}\iota\vartheta - \check{p}\iota), & \frac{\check{p}-2}{2^{k+1}} \le \vartheta \le \frac{\check{p}+2}{2^{k+1}} \\ 0, \text{ otherwise,} \end{cases} \quad (13)$$

Where:

$$\widetilde{L_q} = \begin{cases} \frac{1}{\sqrt{\pi}}, q = 0 \\ \sqrt{\frac{2}{\pi}}L_q(\vartheta), q > 0 \end{cases} \quad (14)$$

Now, S is defined as the maximum order of the Lucas polynomials. The indices for the Lucas polynomials are given by $q = 0, 1, 2, \ldots, S-1$. $\check{p}$ is also defined as $2(2p+1)$, where p takes values from 0 to $2k-1$, with k being any non-negative integer.

The Lucas wavelets, denoted as $Lq(\vartheta)$, are a set of Lucas polynomials of order S that are orthogonal concerning:

$$w(\vartheta) = \frac{1}{\iota\sqrt{\vartheta^4+4}}$$

2.6.4. Function approximation

A function $f(\vartheta)$ defined over the interval [0, 2) can be expanded in terms of Lucas wavelets as follows:

$$f(\vartheta) = \sum_{n=1}^{\infty}\sum_{m=0}^{\infty} c_{nm}\,\psi_{nm}(\vartheta) \quad (15)$$

By truncating the infinite series in Equation (15) concerning the p and q of the Lucas wavelet, then the coefficients c_{nm} represent the values of the function $f(\vartheta)$. The term $\psi_{n,m_{w_k}}$ represents the inner product of $f(\vartheta)$ and $\psi_{nm}(\vartheta)$, where $\psi_{nm}(\vartheta)$ is a Lucas wavelet with a weight function $w(\vartheta)$.

$$f(\vartheta) = f_{2^kS-1}(\vartheta)\sum_{n=1}^{2^k}\sum_{m=0}^{S-1} c_{nm}\,\psi_{nm}(\vartheta) = F^T\psi(\vartheta) \quad (16)$$

Where F and $\psi(t)$ are $2^kS \times 1$ matrices given by:

$$F = [f_{1,0}, f_{1,1}, \ldots, f_{1,S-1}, f_{2,0}, \ldots, f_{2,S-1}, \ldots, f_{2^k,S-1}]^T \quad (17)$$

$$\psi(\vartheta) = [\psi_{1,0}(\vartheta), \psi_{1,1}(\vartheta), \ldots, \psi_{1,S-1}(\vartheta), \psi_{2,0}(\vartheta), \ldots, \psi_{2,S-1}(\vartheta), \ldots, \psi_{2^k,0}(\vartheta), \ldots, \psi_{2^k,S-1}(\vartheta)]^T \quad (18)$$

If $\psi(\vartheta)$ is defined as the Lucas wavelet vector in (Eq. 18), then the first derivative of this vector can be expressed as:

$$\frac{d\psi(\vartheta)}{d\vartheta} = E\psi(\vartheta) \quad (19)$$

Where E is 2^kS square matrix of order the derivative:

$$E = \begin{pmatrix} F & F \\ F & F \end{pmatrix}$$

Here, a square matrix F of order S, where each element in the (μ, δ) position is defined as:

$$F_{\mu,\delta} = \begin{cases} 2^{k+1}\iota(\mu-1)\sqrt{\frac{\alpha_{\mu-1}}{\alpha_{\delta-1}}}, \mu = 2, 3, \ldots, S, \delta = 1, 2, \ldots, \mu-1, \mu+\delta = odd \\ 0, \text{ otherwise} \end{cases} \quad (20)$$

For proof of this theorem, see reference [34].

2.6.5. Corollary [18] and Convergence theorem

DOI: 10.22281/2413-9920-2025-11-04-470-486

The operational matrix of the derivative for an nth-order can be obtained by:

$$\frac{d^n\psi(\vartheta)}{d\vartheta^n} = E^n\psi(\vartheta), \quad n = 1,2,\ldots \quad where\ E^n\ is\ n^{th}\ power\ of\ E.$$

The Lucas wavelet series solution, as defined in (Eq. 15), converges uniformly towards the function $f(\vartheta)$ when Lucas wavelets are utilized [18].

2.6.6. Multi-Layer Perceptron (MLP) approach in wavelet

In this study, a widely recognized feed-forward artificial network known as the Multi-layer Perceptron (MLP) was utilized [35]. It is a powerful tool, capable of expanding the Lucas wavelet domain for roll angle data forecasting. The time-series format of roll angle data is crucial for accurate forecasting, and we assumed that the MLP model's output relies on the last 5 seconds of roll angle history for improved results. The forecasting process, illustrated in Fig. 3, involves formulating roll angle data from the wavelet solution, which is then treated as input for the MLP model's input layer. The network comprises an input, with four hidden layers and an output layer with a sigmoid activation function. Employing the Adam optimizer with an initial value of 0.001 effectively regulates the learning rate of the feed-forward network in the context of wavelet time-series forecasting. With this network configuration, the MLP successfully forecasted the next 50 seconds of roll angle data with a high level of accuracy, evaluated with correlation coefficient $\boldsymbol{R^2}$.

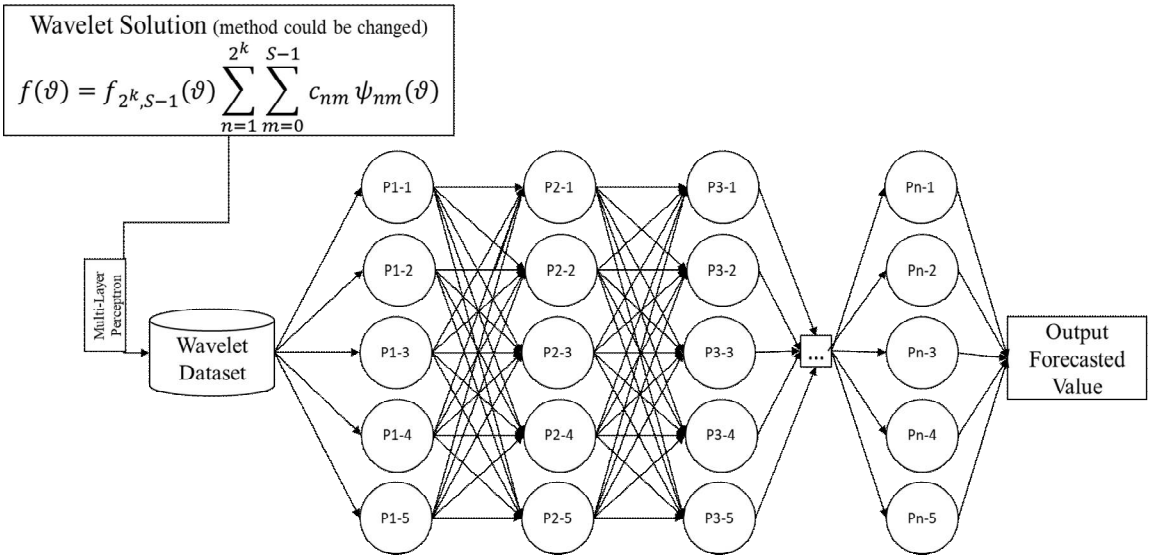

Figure 3. Flowchart of MLP forecasting the roll motion

2.7. Illustrative examples

The study explores cargo ship roll motion using the Lucas Wavelet algorithm, alongside alternative methods like HPM and AGM. By considering damping and restoring moments, the Lucas Wavelet method effectively approximates roll angles. Furthermore, employing MLP with LWM enhances roll angle forecasting, shedding light on the ship's dynamic behavior. Similarly, equations governing ship roll motion, considering linear and quadratic damping, are analyzed, with solutions derived using the Lucas Wavelet method and compared with HPM and AGM solutions. The integration of MLP with LWM offers deeper insights into the ship's roll motion dynamics under different conditions.

2.7.1. Nonlinear roll motion of cargo ship

The equation (4) can also be written as:

$$\frac{d^2\theta}{d\vartheta^2} + b_1\frac{d\theta}{d\vartheta} + b_2\frac{d\theta}{d\vartheta}\left|\frac{d\theta}{d\vartheta}\right| + C_1\theta = 0 \quad (21)$$

With initial conditions defined as: $\theta(0) = \theta_0, \dot{\theta}(0) = 0$

From equation (21), damping moments are set as $b_1 = 0.0238$ and $b_2 = 0.552$. Restoring

DOI: 10.22281/2413-9920-2025-11-04-470-486

moment is also experimentally obtained [31] , and the coefficient of the linear restoring moment is considered to be $C_1 = 0.17528$. The initial conditions for solving (Eq. 21) are as follows:

$$\theta(0) = 0.0698, \dot{\theta}(0) = 0 \quad (22)$$

As solving (Eq. 21) with initial conditions (Eq. 22), using the Lucas Wavelet algorithm, for the case of k=0 and S=3, the approximation results for $\theta(\vartheta)$ is obtained. The two operational metrics E and E^2, are given as:

$$E = \begin{pmatrix} 0 & 0 & 0 \\ t\sqrt{2} & 0 & 0 \\ 0 & 4t & 0 \end{pmatrix} \text{ and } E^2 = \begin{pmatrix} 0 & 0 & 0 \\ 0 & 0 & 0 \\ -4\sqrt{2} & 0 & 0 \end{pmatrix}$$

As the function could be obtained by equation (18), the following relation is applied:

$$\psi(\vartheta) = \sqrt{\frac{2}{\pi}} \begin{pmatrix} 2 \\ 2\iota(\vartheta - 1) \\ (-4\vartheta^2 + 8\vartheta - 2) \end{pmatrix}$$

$$(c_{0,0}, c_{0,1}, c_{0,2})^T = (c_0, c_1, c_2)^T \quad (23)$$

Therefore, the LWM would be given by:

If C is set as

$$C^T D^2\psi(t) + 0.0238C^T D\psi(t) + 0.552C^T (D\psi(t))^2 + 0.17528C^T\psi(t) = 0 \quad (24)$$

If t=1 is chosen to be the collection point, the following equations will be applied:

$$141.312c_2^2 - 10.00185c_2 + 0.01223 = 0 \quad (25)$$

Applying the boundary conditions, we gain:

$$2c_0 - 2\iota c_1 - 2c_2 = 0.0698 \quad (26)$$

$$2\sqrt{2}\iota c_1 + 8c_2 = 0 \quad (27)$$

Solving algebraic equations simultaneously, we obtain:

$$c_0 = 0.0395, c_1 = 0.0034\iota, c_2 = 0.0395$$

By connections coefficients above, the wavelet solution is obtained as:

$$\theta(\vartheta) = 0.0834 - 0.0048\vartheta^2 \quad (28)$$

2.8. Equations governing the ship roll motion

This section investigates the incorporation of both linear and quadratic damping as well as restoring moments. Decay damping coefficients mentioned in Table 3. are also taken from the reference [10]:

$$\frac{d^2\theta}{d\vartheta^2} + b_1\frac{d\theta}{d\vartheta} + b_2\frac{d\theta}{d\vartheta}\left|\frac{d\theta}{d\vartheta}\right| + \omega_n^2\theta = 0 \quad (31)$$

Also, the initial conditions are defined as: $\theta(0) = \theta_0, \dot{\theta}(0) = 0$

Table 3

Decay damping coefficients in different conditions

Condition	Standard condition		Full condition	
	$b_1[s^{-1}]$	$b_2[s^{-1}]$	$b_1[s^{-1}]$	$b_2[s^{-1}]$
Init 5°	-	-	0.020	0.192
Init 10°	0.015	0.710	0.015	0.555
Init 15°	-	-	0.014	0.586
Init 20°	0.018	0.705	-	-

Study Case (I): In this context, (Eq. 31) is examined with fixed coefficients, where the corresponding experimental values are provided in Table 3. for the natural roll period $T_n = 14.8$ seconds.

$$b_1 = 0.015, b_2 = 0.555, \omega_n^2 = 0.18023$$

With conditions as:

$$\varphi(0) = 0.174533, \dot{\varphi}(0) = 0 \quad (32)$$

By employing the Lucas wavelet method's operational matrix approach, we acquire:

DOI: 10.22281/2413-9920-2025-11-04-470-486

$$C^T D^2\psi(t) + 0.015D\psi(t) + 0.555(D\psi(t))^2 + 0.18023C^T\psi(t) = 0 \quad (33)$$

Selecting t = 1 as the collocation point leads to the following equation.

$$141.312c_2^2 - 10.00185c_2 + 0.01223 = 0 \quad (34)$$

Applying the boundary conditions, we gain:

$$2c_0 - 2\iota c_1 - 2c_2 = 0.175433 \quad (35)$$

$$2\sqrt{2}\iota c_1 + 8c_2 = 0 \quad (36)$$

Solving algebraic equations simultaneously, we obtain:

$$c_0 = 0.081835, c_1 = 0.0084\iota, c_2 = 0.00297$$

By connections coefficients above, the wavelet solution is obtained as:

$$\theta(\vartheta) = 0.175433 - 0.00146\vartheta^2 \quad (37)$$

The HPM solution is obtained as:

$$\theta(\vartheta) = (e^{-0.075\vartheta}((0.0030838\ sin(0.424469\vartheta) + (0.175433\ cos(0.424469\vartheta) \quad (38)$$

The AGM solution is obtained as:

$$\theta(\vartheta) = (e^{-6.95393\vartheta}((-8.237253.10^{-9} sin(37.8899\vartheta) + (0.174519968\ cos(0.422796\vartheta) \quad (39)$$

And also, the MLP - LWM gives the roll angle solution.

Study Case (II): In this context, (Eq. 39) is examined with fixed coefficients, where the corresponding experimental values are provided in Table 3 for the natural roll period $T_n = 14.44$ seconds.

$$b_1 = 0.015, b_2 = 0.710, \omega_n^2 = 0.19039$$

With conditions such as:

$$\varphi(0) = 0.174533, \dot{\varphi}(0) = 0 \quad (40)$$

By employing the Lucas wavelet method's operational matrix approach, we acquire:

$$C^T D^2\psi(t) + 0.015C^T D\psi(t) + 0.71C^T(D\psi(t))^2 + 0.19039C^T\psi(t) = 0 \quad (41)$$

Selecting t = 1 as the collocation point leads to the following equation.

$$181.76c_2^2 - 11.86916c_2 + 0.03322 = 0 \quad (42)$$

Applying the boundary conditions, we gain:

$$2c_0 - 2\iota c_1 - 2c_2 = 0.175433 \quad (43)$$

$$2\sqrt{2}\iota c_1 + 8c_2 = 0 \quad (36)$$

Solving algebraic equations simultaneously, we obtain:

$$c_0 = 0.081908, c_1 = 0.00828\iota, c_2 = 0.00293$$

By connections coefficients above, the wavelet solution is obtained as:

$$\theta(\vartheta) = 0.175433 - 0.00156\vartheta^2 \quad (44)$$

The HPM solution is obtained as:

$$\theta(\vartheta) = (e^{-0.075\vartheta}((0.003004\ sin(0.436237\vartheta) + (0.175433\ cos(0.436237\vartheta) \quad (45)$$

The AGM solution is obtained as:

$$\theta(\vartheta) = (e^{0.005\vartheta}((-7.3941351.10^{-10} sin(68.66396\vartheta) + (0.000111\ cos(1.69391\vartheta) \quad (46)$$

And also, the MLP - LWM gives the roll angle solution.

3. RESULTS AND DISCUSSION

The MLP - LWM model trained for wavelet roll-damping prediction initially exhibits poor performance for the lower number of epochs with negative R^2 values, indicating a lack of correlation between predicted and actual values. However, through successive epochs, the model demonstrates significant improvement, gradually increasing its R^2 values until they approach near unity. The final forecasted value aligns well with expectations, suggesting the model's ability to capture underlying patterns effectively. This progression underscores the MLP's capacity to learn complex relationships within the data and highlights its potential for accurate prediction in wavelet roll-damping scenarios. The progression for training and evaluations

DOI: 10.22281/2413-9920-2025-11-04-470-486

through R^2 values are mentioned in Table 4. The forecasted values are provided further.

Table 4

Epochs and Correlation Coefficient of the MLP – LWM

Epoch	R^2
1	-18.126725
51	-0.059608
101	0.000619
151	0.001585
201	0.002340
251	0.003305
301	0.004613
351	0.006473
401	0.009242
451	0.013572
501	0.020766
551	0.033714
601	0.059584
651	0.118084
701	0.264561
751	0.601284
801	0.955520
851	0.998010
901	0.998168
951	0.998191

The comparison of the four mentioned methods: AGM, HPM, MLP - LWM, can give us valuable information. The comparison of methods response to the problem for the Roll angle of 4° illustrated in Fig. 4 as curves and in Fig. 5 as a Scatter plot with error bars.

As may be seen in Table 5, statistical data regarding the mean roll angle (θ) obtained through different methods, along with their standard deviations and error percentages from the AGM (Assumed Ground Model) are presented. Since the AGM is assumed as the reference, there's no error percentage listed for it. The HPM shows a slightly higher mean roll angle compared to the AGM, with an error percentage of 0.87%. The MLP - LWM exhibits the highest mean roll angle among the methods compared to the AGM, with an error percentage of 5.11%, this may be showcasing the fact that the MLP - LWM model requires further hyperparameter tuning, or even more wavelet data to be trained with.

As may be seen in Fig.4, The graph depicts the decay of Theta (θ) over time (t) for three different methods: AGM, HPM, and MLP-LWM. All methods show a decreasing trend, with MLP-LWM exhibiting the most rapid decay, followed by AGM and HPM. Error Percentage and Standard Deviation from AGM are given in Table 5.

Fig 5. illustrates the oscillation of Theta (θ) over time (t) for three methods: AGM, HPM, and MLP-LWM. AGM and HPM exhibit similar results, while MLP-LWM provides the closest approximation to the true signal, capturing even the smallest noise components in roll-damping angle prediction.

DOI: 10.22281/2413-9920-2025-11-04-470-486

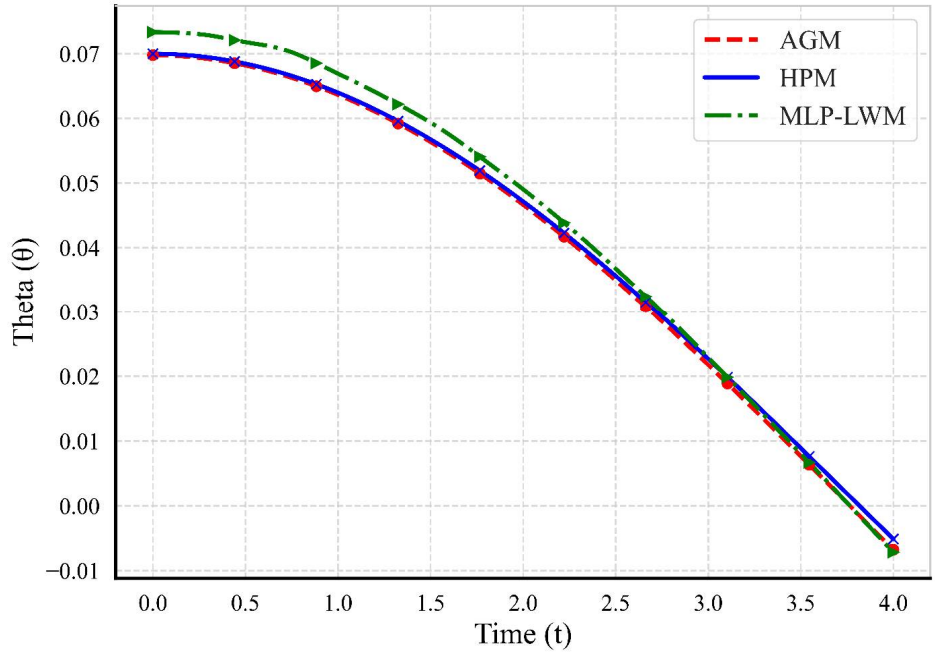

Figure 4. Comparative curve of AGM, HPM, and MLP - LWM for Roll angle of 4°

Table 5

Error Percentage and Standard Deviation from AGM

Method	Mean Theta (θ)	Std Deviation	Error Percentage from AGM
AGM	0.0528	0.0146	-
HPM	0.0532	0.0145	0.87%
MLP - LWM	0.0555	0.0154	5.11%

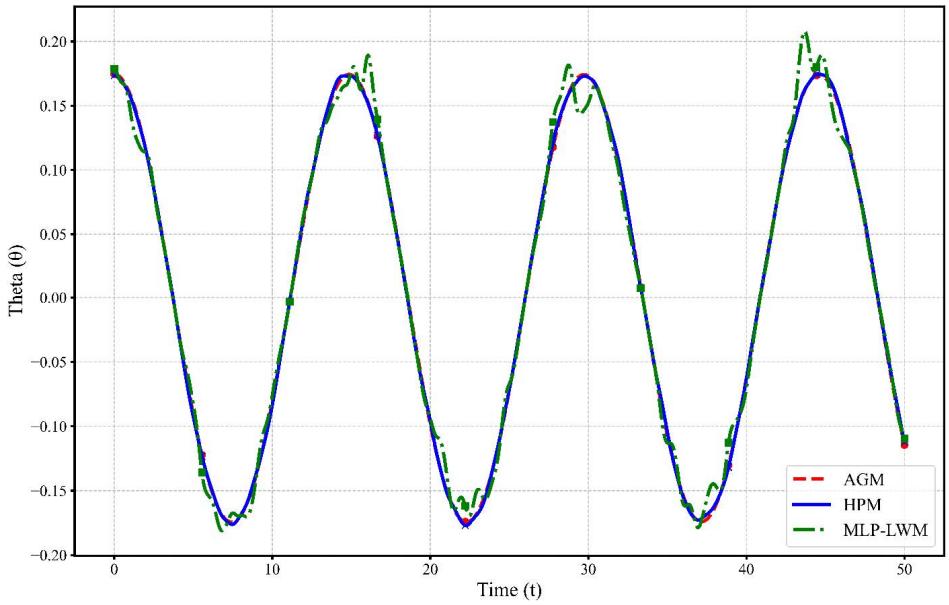

Figure 5. Case Study (I) Comparative study of AGM, HPM, and MLP - LWM for Roll angle of 4°

DOI: 10.22281/2413-9920-2025-11-04-470-486

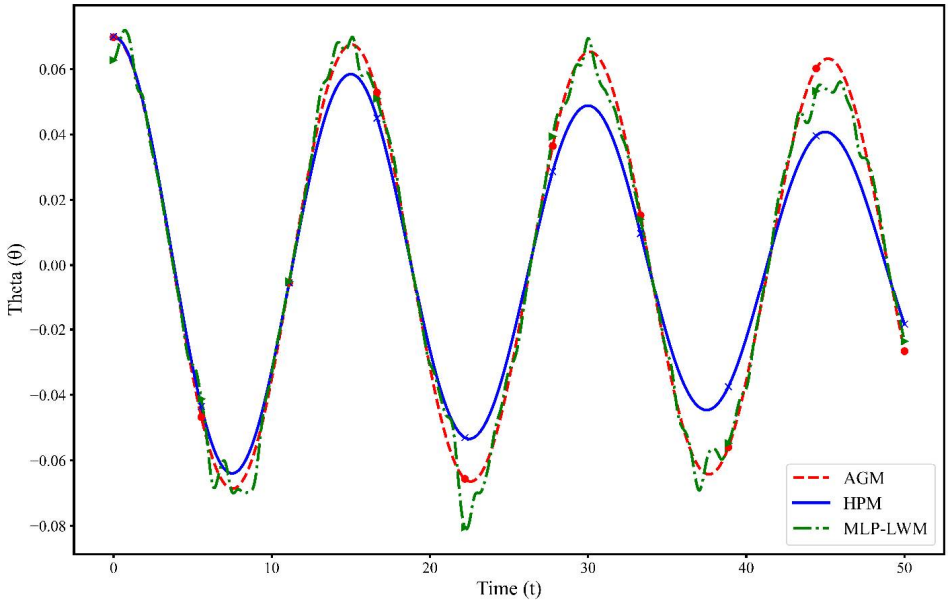

Figure 6. Case Study (II) Comparative study of AGM, HPM, and MLP - LWM for Roll angle of 4^{0}

Table 6

Comparison of Methods over time for Cases I and II

Case	Case Study (I)			Case Study (II)		
Time (s)	AGM	HPM	MLP-LWM	AGM	HPM	MLP-LWM
0.00	0.1745	0.1776	0.1717	0.1745	0.1748	0.1867
0.44	0.1714	0.1746	0.1686	0.1714	0.1717	0.1833
0.89	0.1623	0.1654	0.1596	0.1623	0.1626	0.1735
1.33	0.1475	0.1506	0.1450	0.1475	0.1478	0.1575
1.78	0.1275	0.1306	0.1253	0.1275	0.1278	0.1361
2.22	0.1030	0.1061	0.1011	0.1030	0.1033	0.1098
2.67	0.0748	0.0779	0.0735	0.0748	0.0751	0.0798
3.11	0.0441	0.0472	0.0433	0.0441	0.0444	0.0470
3.56	0.0118	0.0148	0.0116	0.0118	0.0121	0.0125
4.00	-0.0210	-0.0179	-0.0206	-0.0210	-0.0207	-0.0223

Fig 6. displays the oscillation of Theta (θ) over time (t) for three methods: AGM, HPM, and MLP-LWM. All methods exhibit approximately the same pattern, with MLP-LWM capturing the fine details and amplitude variations more closely to AGM than HPM.

Table 5 and the following Fig 7. present a comparison of three methods (AGM, HPM, and MLP-LWM). The results are displayed over time, with the dependent variable denoted as "Theta (θ)".

All three methods generally follow a decreasing trend over time, suggesting a decay or damping behavior in the underlying case studies. At the initial time step (t=0), all three methods produce similar values for Theta, indicating a consistent starting point.

AGM and HPM: These methods exhibit relatively close results throughout the time span, suggesting similar levels of accuracy.

MLP-LWM: This method often produces slightly higher values than AGM and HPM, indicating more accurate pattern recognition. The slight deviations of MLP-LWM might be attributed to differences in its learning curve or implementation.

DOI: 10.22281/2413-9920-2025-11-04-470-486

The analysis of two case studies, each comprising data from three models -AGM, HPM, and MLP - LWM reveals distinct trends. In Case Study (I), all models commence with comparable values at time 0.00, but as time progresses, AGM consistently maintains higher values compared to HPM and MLP - LWM. Moreover, the values for all models decrease over time intervals, with AGM consistently outperforming the other models. Similarly, in Case Study (II), AGM exhibits higher values from the onset, maintaining its superiority over HPM and LWM throughout the observation period. The patterns observed in Case Study (II) mirror those in Case Study (I), with AGM consistently surpassing the other models in terms of value retention over time. Thus, the Average Growth Model emerges as the most effective among the three models analyzed, demonstrating its superiority in maintaining higher values across various time intervals in both case studies.

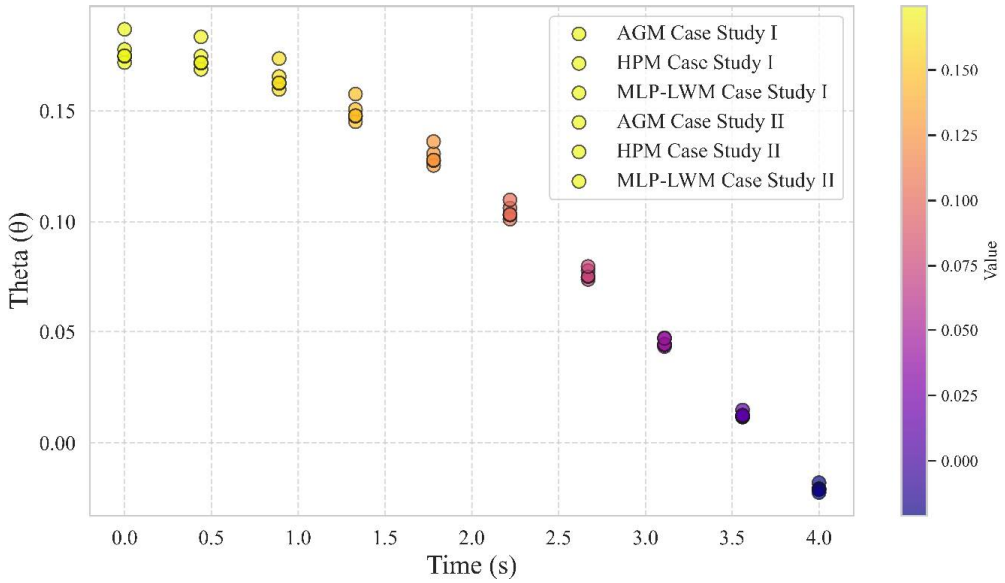

Figure 7. Scatter Plot with Color Mapping for Case Studies

4. Conclusion

In this study, the performance of the MLP-LWM model for predicting wavelet roll-damping and compared it with the AGM and HPM models was investigated. The results highlight the ability of the MLP-LWM model to improve over time, with R^2 values rising from negative to near unity as the training epochs progressed, demonstrating its potential to capture complex relationships in the data. However, despite these improvements, the MLP-LWM model showed higher error percentages (5.11%) compared to the AGM (0%) and HPM (0.87%), indicating that it is less accurate in its current form.

The comparative analysis of roll angle predictions reveals that the AGM model consistently outperforms the others in terms of accuracy and stability, with the most reliable results observed in both case studies. The HPM performed slightly better than MLP-LWM but still lagged behind AGM. The MLP-LWM model, while effective in capturing finer details, requires further hyperparameter tuning and additional training data to improve its prediction accuracy.

Overall, the AGM remains the most effective model for wavelet roll-damping prediction in this study. However, the MLP-LWM model shows promise and, with further refinement, could offer valuable insights and improvements for more complex wave-damping scenarios. Future work will focus on enhancing the MLP-LWM model's performance through better training techniques and data augmentation, aiming to close the accuracy gap with the AGM.

Future Work

Potential future avenues for research in ship roll-damping prediction could involve the de-

DOI: 10.22281/2413-9920-2025-11-04-470-486

velopment and exploration of advanced AI models, specifically focusing on weakly supervised or unsupervised learning techniques. Leveraging the power of machine learning algorithms to discern patterns and relationships within the vast datasets associated with maritime dynamics could enhance prediction accuracy. Additionally, there is scope for the creation of a model capable of intelligently selecting the most appropriate non-linear solution for each specific roll-damping problem based on its inherent physics and nature. This would involve a comprehensive understanding of the underlying dynamics, enabling the model to adapt and choose the most accurate prediction method tailored to the unique characteristics of each scenario. Such an approach would not only contribute to improved accuracy in roll-damping predictions but also offer a more versatile and adaptive solution to the intricacies of maritime operations.

REFERENCES

1. Lalli, F., et al., *A numerical model for wave-current interaction at the scale of marine engineering.* Journal of Operational Oceanography, 2016. **9**(sup1): p. s215-s222.
2. Himeno, P.Y., *Prediction of Ship Roll Damping - state of the Art*. 1981.
3. Taylan, M., *Solution of the nonlinear roll model by a generalized asymptotic method.* Ocean Engineering, 1999. **26**(11): p. 1169-1181.
4. Taylan, M., *The effect of nonlinear damping and restoring in ship rolling.* Ocean Engineering, 2000. **27**(9): p. 921-932.
5. Falzarano, J., Somayajula, Abhilash, & Seah, Robert, *An overview of the prediction methods for roll damping of ships.* Ocean Engineering, 2015. **5(2)**: p. 55-76.
6. Jiang, Y. and R.W. Yeung, *Bilge-Keel Influence on Free Decay of Roll Motion of a Realistic Hull1.* Journal of Offshore Mechanics and Arctic Engineering, 2017. **139**(4).
7. Zhao, W. and F. McPhail, *Roll response of an LNG carrier considering the liquid cargo flow.* Ocean Engineering, 2017. **129**: p. 83-91.
8. Sun, J., S.-L. James Hu, and H. Li, *Nonlinear roll damping parameter identification using free-decay data.* Ocean Engineering, 2021. **219**: p. 108425.
9. Igbadumhe, J.-F., et al. *Experimental Determination of Non-Linear Roll Damping of an FPSO Pure Roll Coupled with Liquid Sloshing in Two-Row Tanks*. Journal of Marine Science and Engineering, 2020. **8**, DOI: 10.3390/jmse8080582.
10. Rodríguez, C.A., et al., *Realistic estimation of roll damping coefficients in waves based on model tests and numerical simulations.* Ocean Engineering, 2020. **213**: p. 107664.
11. Kianejad, S., et al., *Calculation of ship roll hydrodynamic coefficients in regular beam waves.* Ocean Engineering, 2020. **203**: p. 107225.
12. Rezazadeh, N., et al. *Classification of Unbalanced and Bowed Rotors under Uncertainty Using Wavelet Time Scattering, LSTM, and SVM*. Applied Sciences, 2023. **13**, DOI: 10.3390/app13126861.
13. Bernal-Colio, V.R., J. Gómez-Goñi, and J.L. Cercos-Pita, *CFD computation of the hydrodynamic torque due to free-surface antiroll tanks with 3D dynamics.* Ships and Offshore Structures, 2021. **16**(8): p. 879-891.
14. Rostami, A., et al., *Investigating Jeffery-Hamel flow with high magnetic field and nanoparticle by HPM and AGM.* 2014. **4**(4): p. 357-370.
15. Akbari, M.R., et al., *Significant progress in solution of nonlinear equations at displacement of structure and heat transfer extended surface by new AGM approach.* Frontiers of Mechanical Engineering, 2014. **9**(4): p. 390-401.
16. Fard, M.S., et al., *Investigating the magnetohydrodynamics non-Newtonian fluid movement on a tensile plate affected by variable thickness with dufour and soret effects: Akbari Ganji*

DOI: 10.22281/2413-9920-2025-11-04-470-486

and finite element methods. International Journal of Electrochemical Science, 2024. **19**(8): p. 100701.
17. Jalili, B., et al., *The magnetohydrodynamic flow of viscous fluid and heat transfer examination between permeable disks by AGM and FEM.* Case Studies in Thermal Engineering, 2023. **45**: p. 102961.
18. Nourazar, S., M. Soori, and A. Nazari-Golshan, *On the Exact Solution of Burgers-Huxley Equation Using the Homotopy Perturbation Method.* Journal of Applied Mathematics and Physics, 2015. **03**: p. 285-294.
19. domiri ganji, D., Z. Ziabakhsh-Ganji, and H. Ganji, *Determination of temperature distribution for annular fins with temperature dependent thermal conductivity by HPM.* Thermal Science, 2011. **15**.
20. Fathollahi, R., et al., *Analyzing the effect of radiation on the unsteady 2D MHD Al2O3-water flow through parallel squeezing sheets by AGM and HPM.* Alexandria Engineering Journal, 2023. **69**: p. 207-219.
21. Jakeer, S. and B.A.R. Polu, *Homotopy perturbation method solution of magneto-polymer nanofluid containing gyrotactic microorganisms over the permeable sheet with Cattaneo–Christov heat and mass flux model.* Proceedings of the Institution of Mechanical Engineers, Part E: Journal of Process Mechanical Engineering, 2021. **236**(2): p. 525-534.
22. Lepik, Ü., *Numerical solution of differential equations using Haar wavelets.* Mathematics and Computers in Simulation, 2005. **68**(2): p. 127-143.
23. Venkatesh, S.G., S.K. Ayyaswamy, and S. Raja Balachandar, *Legendre Wavelets based approximation method for solving advection problems.* Ain Shams Engineering Journal, 2013. **4**(4): p. 925-932.
24. Idrees, S. and U. Saeed, *Vieta–Lucas wavelets method for fractional linear and nonlinear delay differential equations.* Engineering Computations, 2022. **39**(9): p. 3211-3231.
25. Kumar, R., R. Koundal, and K. Srivastava, *New wavelet method based on Shifted Lucas polynomials: A tau approach.* arXiv preprint arXiv:2003.00778, 2020.
26. Alexandridis, A.K. and A.D. Zapranis, *Wavelet neural networks: A practical guide.* Neural Networks, 2013. **42**: p. 1-27.
27. Esen, H., et al., *Artificial neural network and wavelet neural network approaches for modelling of a solar air heater.* Expert Systems with Applications, 2009. **36**(8): p. 11240-11248.
28. Jun, Z., et al., *Wavelet neural networks for function learning.* IEEE Transactions on Signal Processing, 1995. **43**(6): p. 1485-1497.
29. Swaminathan, G., et al., *A wavelet approximation method for solving nonlinear ship roll damping equations: An operational matrix of derivative approach.* Ocean Engineering, 2022. **264**: p. 112390.
30. Zhao, W., F. McPhail, and M. Efthymiou, *Effect of Partially Filled Spherical Cargo Tanks on the Roll Response of a Bargelike Vessel.* Journal of Offshore Mechanics and Arctic Engineering, 2016. **138**(3).
31. Zhao, W., et al., *Nonlinear roll damping of a barge with and without liquid cargo in spherical tanks.* Journal of Ocean Engineering and Science, 2016. **1**(1): p. 84-91.
32. Roberts, J.B., *Estimation of Nonlinear Ship Roll Damping from Free-Decay Data.* Journal of Ship Research, 1985. **29**(02): p. 127-138.
33. Mohammadi, F. and M.M. Hosseini, *A new Legendre wavelet operational matrix of derivative and its applications in solving the singular ordinary differential equations.* Journal of the Franklin Institute, 2011. **348**(8): p. 1787-1796.
34. Horng, I.-R. and J.-H. Chou, *Shifted Chebyshev direct method for solving variational problems.* International Journal of Systems Science, 1985. **16**(7): p. 855-861.

DOI: 10.22281/2413-9920-2025-11-04-470-486

35. Gardner, M.W. and S.R. Dorling, *Artificial neural networks (the multilayer perceptron)—a review of applications in the atmospheric sciences.* Atmospheric Environment, 1998. **32**(14): p. 2627-2636.